ARMY RESEARCH LABORATORY

Non-destructive Damping Measurement for Wafer-level Packaged Microelectromechanical System (MEMS) Acceleration Switches

by Ryan Knight and Evan Cheng

ARL-TR-7094 September 2014

NOTICES

Disclaimers

The findings in this report are not to be construed as an official Department of the Army position unless so designated by other authorized documents.

Citation of manufacturer's or trade names does not constitute an official endorsement or approval of the use thereof.

Destroy this report when it is no longer needed. Do not return it to the originator.

Army Research Laboratory
Adelphi, MD 20783-1138

ARL-TR-7094 **September 2014**

Non-destructive Damping Measurement for Wafer-level Packaged Microelectromechanical System (MEMS) Acceleration Switches

Ryan Knight and Evan Cheng
Sensors and Electron Devices Directorate, ARL

REPORT DOCUMENTATION PAGE

Form Approved
OMB No. 0704-0188

1. REPORT DATE *(DD-MM-YYYY)*	2. REPORT TYPE	3. DATES COVERED (From - To)
September 2014	Final	

4. TITLE AND SUBTITLE
Non-destructive Damping Measurement for Wafer-level Packaged Microelectromechanical System (MEMS) Acceleration Switches

5a. CONTRACT NUMBER

5b. GRANT NUMBER

5c. PROGRAM ELEMENT NUMBER

6. AUTHOR(S)
Ryan Knight and Evan Cheng

5d. PROJECT NUMBER

5e. TASK NUMBER

5f. WORK UNIT NUMBER

7. PERFORMING ORGANIZATION NAME(S) AND ADDRESS(ES)
U.S. Army Research Laboratory
ATTN: RDRL-SER-L
2800 Powder Mill Road
Adelphi, MD 20783-1138

8. PERFORMING ORGANIZATION REPORT NUMBER
ARL-TR-7094

9. SPONSORING/MONITORING AGENCY NAME(S) AND ADDRESS(ES)

10. SPONSOR/MONITOR'S ACRONYM(S)

11. SPONSOR/MONITOR'S REPORT NUMBER(S)

12. DISTRIBUTION/AVAILABILITY STATEMENT
Approved for public release; distribution unlimited.

13. SUPPLEMENTARY NOTES

14. ABSTRACT
Microelectromechanical systems (MEMS) three-axis acceleration threshold sensors have been developed to measure acceleration threshold levels using voltage switching when the threshold is reached. Determining damping coefficients is important for categorizing how each threshold sensor or switch operates. Switches with different damping coefficients result in different mechanical impedances and response times. Analytical and numerical methods to model damping coefficient values based on empirical data are needed to characterize three-axis acceleration sensors; traditional methods use the displacement of an underdamped system to calculate the damping ratio. Mechanical switches are single output devices that distinguish whether closure occurs or not and lack a transduction mechanism to turn acceleration into a readable displacement signal. Thus, we have devised a more inventive technique to analyze a closed switch. A shock table and vibration testing produces a deterministic acceleration input to close an acceleration switch, which has a defined switch gap distance, and mathematical fitting using these deterministic values allows one to determine damping coefficients. By using both an analytical equation fit method and a numerical optimization program, the damping coefficients for MEMS three-axis threshold acceleration sensors were calculated from the results of the tests and design dimensions of the switches.

15. SUBJECT TERMS
MEMS acceleration impact switch damping coefficient response

16. SECURITY CLASSIFICATION OF:			17. LIMITATION OF ABSTRACT	18. NUMBER OF PAGES	19a. NAME OF RESPONSIBLE PERSON
a. REPORT	b. ABSTRACT	c. THIS PAGE			Ryan Knight
Unclassified	Unclassified	Unclassified	UU	38	19b. TELEPHONE NUMBER (*Include area code*) 301-394-3710

Contents

List of Figures

List of Tables

INTENTIONALLY LEFT BLANK.

1. Introduction/Background

Mechanical analysis of microelectromechanical system (MEMS) acceleration switches has been successfully modeled based off of Newtonian dynamic equations of motion.[1] Damping plays an important part in varying the response of MEMS acceleration switches and is an integral part of system modeling. In isolated environments filled with a working fluid that dissipates energy, damping between parallel and sliding plates that are affected by compression forces and internal friction cause energy loss and is often referred to as squeeze-film and Couette damping.[2] Reynolds equations have been applied to model the squeeze-film air damping in MEMS switches. The Reynolds number for MEMS is especially small due to extremely small geometries and inertial forces are often negligible, so the behavior of fluids is based primarily on the viscous effects.[3]

Experimental evaluations of MEMS systems required modeling damping by evaluating displacement or oscillation using piezoelectric, electromagnetic, or electrostatic (capacitive sensing) transduction mechanisms.[4,5] A previous study determined damping in oscillating cantilever tuning forks by linearizing the Reynolds equation at a set gap distance.[6] Other studies measured the oscillation amplitude at resonant frequencies and estimated the values from the logarithmic decrement of those amplitudes.[7,8] Experiments that did not rely on resonant frequencies used capacitance measurements or pressure sensors to relate changes in capacitance or pressure directly to displacement. The analytical methods and experimental methods for these studies all consisted of differentiation of measured displacement to calculate damping forces.[9,10]

Previous reported studies were only able to determine damping by measuring displacement. The data for isolated MEMS acceleration threshold sensor or switches are limited because switch closure only quantifies single instances of voltage change (i.e., switch closure). Two novel methods are discussed as non-destructive methods for damping measurement of wafer-level packaged MEMS contact switches. The first uses empirical acceleration table results and modeling a second-order-differential-equation fit to mimic the MEMS acceleration switch response. This method iteratively adjusts the damping ratio until the solution converges.

The second method uses harmonic vibration empirical data to solve the amplification ratio equation for both natural frequency and damping. The MEMS acceleration switch is vibrated at an amplitude where the switch begins to make closure at its natural frequency. The frequency span window values where switch closure first occurs and finally opens are the ends points for solving a nonlinear amplification ratio equation. This method is constrained to solve only underdamped systems; however, it is more advantageous when quantifying single modal damping values rather than impact excitation where many modes are excited.

The two damping measurement techniques presented are unique in their application and cover all damping ratio values: underdamped and overdamped systems. Damping characterization will benefit end users by allowing a framework for modeling acceleration switch response in their application and help them correctly choose a closure-acceleration value for the MEMS switch.

1.1 Equations of Motion

A linear shock table was used to test the sensors, allowing the data acquisition device to plot acceleration and voltage change over time. An open switch indicated little or no voltage drop, but at switch closure, the short circuit caused a change in voltage. In Fig. 1, the voltage was measured against time, and the change in voltage corresponded to the g-force at the time of switch closure. The acceleration and voltage change was analyzed with the system modeled as a mass with a spring and damper in a second-order differential equation.

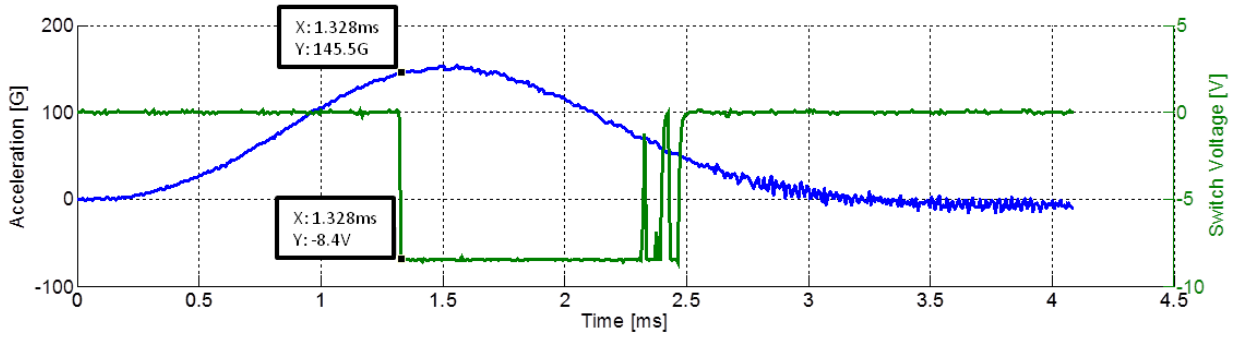

Fig. 1 Example of the data taken by the data acquisition device

The impact table will produce high amplitude shocks and will terminate the motion with shock absorbers. The resulting acceleration forms a half-sine curve, which is applied as a driving function in the equation of motion. The governing differential equation for the motion of the proof mass is given by Eq. 1

$$m\ddot{x}(t) + c\dot{x}(t) + kx(t) = F\sin(\omega t) \tag{1}$$

or Eq. 2 in displacement form

$$\ddot{x}(t) + 2\zeta\omega_n\dot{x}(t) + \omega_n^2 x(t) = \frac{F}{m}\sin(\omega t) \tag{2}$$

where m is the mass (kg), c is the damping coefficient, k is the spring constant (N/m), F is the driving force (N) (defined by Newton's law $\sum F = ma$), ζ is the damping coefficient

$$\zeta = \frac{c}{2\sqrt{km}} \tag{3}$$

and ω_n is the natural frequency (rad/s)

$$\omega_n = \sqrt{\frac{k}{m}} \tag{4}$$

The general form of the solution to the system, assuming a harmonic driving function and an underdamped system, is given by

$$x(t) = e^{-\zeta\omega_n t}[c_1 \cos(\omega_d t) + c_2 \sin(\omega_d t)] + R \sin(\omega t - \varphi) \tag{5}$$

where c_1 and c_2 are displacement coefficients of the terms of the transient solution obtained from the initial conditions (initial displacement and initial velocity is at zero), ω is the harmonic frequency (rad/s), ω_d is the damping frequency (rad/s)

$$\omega_d = \omega_n\sqrt{1-\zeta^2} \tag{6}$$

and R is the coefficient of the steady state solution Eq. 2 derived by substituting the steady-state component into the equation of motion

$$R = \frac{F/_k}{\sqrt{\left[1-\left(\frac{\omega}{\omega_n}\right)^2\right]^2 + \left[2\zeta\left(\frac{\omega}{\omega_n}\right)\right]^2}} \tag{7}$$

and phase angle, φ, is

$$\varphi = \tan^{-1}\left[\frac{\frac{2\zeta\omega}{\omega_n}}{1-\left(\frac{\omega}{\omega_n}\right)^2}\right] \tag{8}$$

Solving the equation for c_1 and c_2 using the initial conditions results in the real part of the solution

$$x(t) = e^{-\zeta\omega_n t}\left[R\,sin(\varphi)\,cos(\omega_d t) + R\,\frac{[\zeta\omega_n\,sin(\varphi) - \omega\,cos(\varphi)]}{\omega_d}sin(\omega_d t)\right] + R\,sin(\omega t - \varphi) \tag{9}$$

The vibration and impact empirical data discussed in Section 1.3.2 analyzes two forms of Eq. 9, $t \ll 1$ and $t \gg 1$.

$$x(t \ll 1) = e^{-\zeta\omega_n t}\left[R\sin(\varphi)\cos(\omega_d t) + R\,\frac{(\zeta\omega_n\sin(\varphi) - \omega\cos(\varphi))}{\omega_d}\sin(\omega_d t)\right] + R\sin(\omega t - \varphi) \tag{10}$$

$$x(t \gg 1) = \frac{F/_k \sin(\omega t - \varphi)}{\sqrt{\left[1-\left(\frac{\omega}{\omega_n}\right)^2\right]^2 + \left[2\zeta\left(\frac{\omega}{\omega_n}\right)\right]^2}} \tag{11}$$

Dividing the output $x(t)$ by the input leads to the amplification ratio for a harmonic second-order system

$$\frac{x_o}{x_i} = \frac{1}{\sqrt{\left[1-\left(\frac{\omega}{\omega_n}\right)^2\right]^2 + \left[2\zeta\left(\frac{\omega}{\omega_n}\right)\right]^2}} \tag{12}$$

Equation 12 can be solved for ω_n and ζ given that x_o, x_i, and the respective ω's are known.

1.2 Squeeze-Film Damping

Squeeze-film air damping, as shown in Fig. 2, is created by the compressing the gas between two surfaces moving at a certain decreasing gap distance and creating a resistant force to the movement. The damping pressure between two plates consists of a viscous damping force and an elastic damping force.

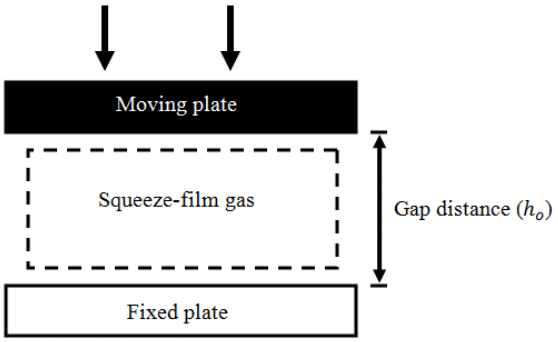

Fig. 2 Squeeze-film air damping between a moving plate and a fixed plate

In cases of high frequency oscillations, the elastic force dominates the viscous force and is proportional to the displacement of the plate. The coefficient of the elastic damping force $k_e(\sigma)$ as determined by Bao and Yang[3] is described as

$$k_e(\sigma) = \frac{64\sigma^2 P_a A}{\pi^8 h_o} \sum_{m,n\ \text{odd}} \frac{1}{(mn)^2\left\{\left[m^2 + \left({}^{n}/_{\eta}\right)^2\right]^2 + {}^{\sigma^2}/_{\pi^4}\right\}} \tag{13}$$

where P_a is the ambient pressure (Pa), A is the area of the plate (m^2), η is the aspect ratio of the plate (for a square plate, $\eta = 1$), and σ is the squeeze number given by

$$\sigma = \frac{12\mu\omega l^2}{P_a h_o^2} \tag{14}$$

where μ is the coefficient of viscosity of the gas (Pa-s), and l is the characteristic length of the plate (m).[3] As shown in Eqs. 13 and 14, greater force between the two plates will be caused by a

higher squeeze number, which can be designedly caused by increasing characteristic length or decreasing the gap distance. The equation of motion is then be described as

$$m\ddot{x}(t) + c\dot{x}(t) + (k + k_e)x(t) = F\sin(\omega t) \tag{15}$$

Equation 15 can be solved for the damping coefficient given the input forcing function and known input design parameters, m, $k + k_e$, and gap distance when the acceleration switch closes.

1.3 Analysis Methods

Two methods were developed that characterize the damping ratio for packaged MEMS acceleration switches. MEMS acceleration switches only provide a single point of information in an applied acceleration field—when switch closure occurs. Other MEMS devices use transducers like capacitive, piezoelectric, optical, and pressure to discern a continuous displacement signal. Knowing displacement as a function of time allows for damping to be calculated via the classical ring-down log decrement technique. Additionally, the damping ratio for underdamped systems can be predicted by the frequency response to a harmonic excitation using the –3 dB rule. These two methods are frequently used to characterize damping for micro-devices. When displacement is no longer continuously known, for example, in MEMS acceleration switches, traditional techniques to measure damping can no longer be applied. The two methods discussed below are ways to measure damping when switch closure is all that is known.

1.3.1 Analysis Methods 1: Acceleration Table Damping Predictor

The analytic method used the solution for the equations of motion Eq. 9 to compute the damping coefficient at the time of specified voltage changes. MEMS acceleration switches developed for 60G fuzing impact environments were used to evaluate the non-destructive method for damping measurement. The Department of Defense's Joint Fuze Technology Program (JFTP) provided the funding behind the production of the 60G MEMS impact switches. The JFTP MEMS impact switches are omnidirectional, consisting of two out-plane contact (top and bottom) and one in-plane contact for lateral or side acceleration events. Figure 3 illustrate the computer-aided design (CAD) layout for the 60G MEMS acceleration switches. For the top and bottom contacts of the JFTP 60G sensors, the squeeze-film air damping was taken into account due to the rectangular plate design.

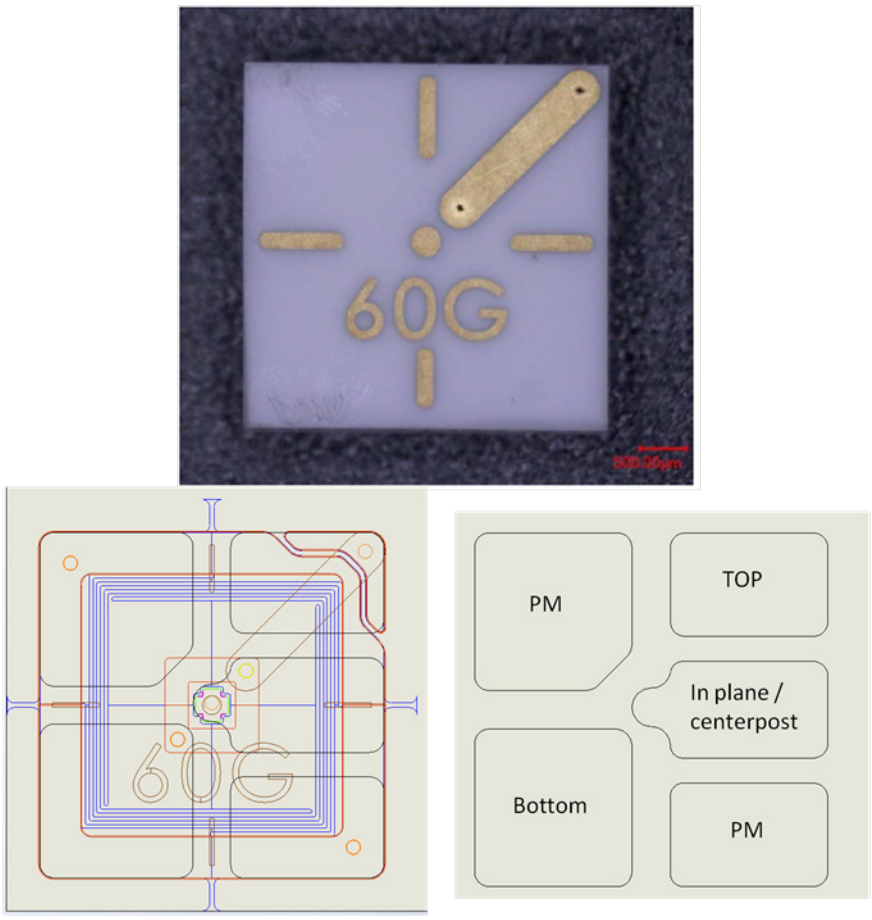

Fig. 3 MEMS JFTP 60G impact switch layout

The numerical method approximated the damping by first estimating a damping coefficient value and then comparing the time value at the determined damping to the actual time of switch closure. By adjusting the time value until it was equivalent to the time of switch closure and modifying the damping coefficient value accordingly, the damping coefficient value for the function was determined at the instance of voltage changes.

1.3.2 Analysis Methods 2: Harmonic Excitation Modal Damping Predictor

To evaluate the harmonic excitation modal damping predictor (HEMDP) method, underdamped 50–2000G MEMS impact acceleration switches were tested. These switches were chosen because they were known to be underdamped, which is needed for the prescribed method. The JFTP 60G impact switch was designed to have higher damping and given that it's a relatively new device the damping values were unknown and, hence, not used for HEMDP test setup.

The 50–2000G MEMS impact switches used in fuzing applications were mounted to an inductive shaker and vibrated at constant amplitude for sine sweeps with frequencies ranging from 100 Hz–10 kHz. The switches are omnidirectional; therefore, switch closure is dependent

upon switch orientation during vibration. Figure 4 illustrate the 50G omnidirectional acceleration switch with its lid removed.

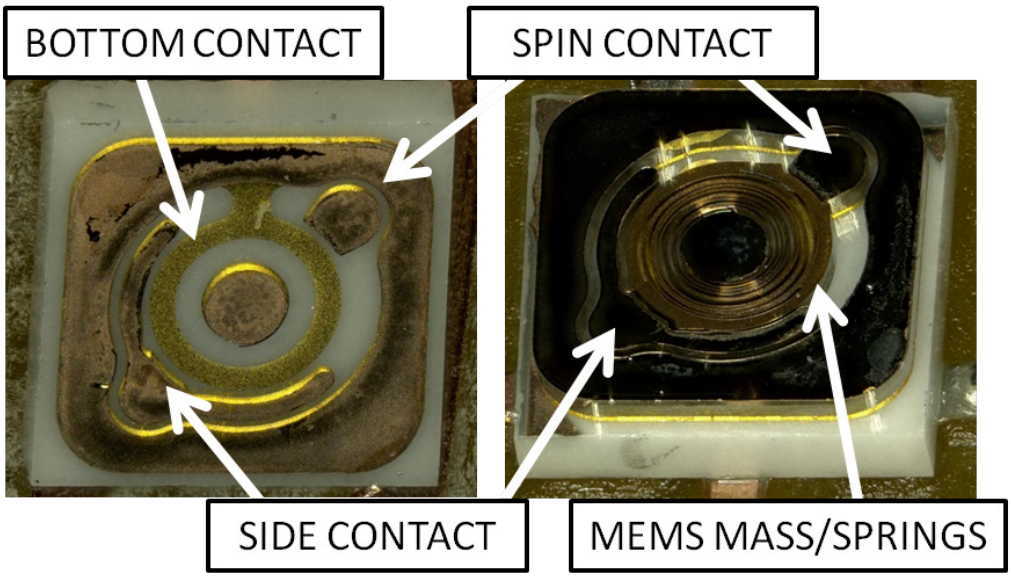

Fig. 4 The 50G MEMS acceleration switch with its lid removed

Modal frequency separation is large enough that modal coupling effects can be ignored. The MEMS impact switches were evaluated both in the ±z out-of-plane and in the orthogonal planar direction.

The modal damping values are evaluated by using the harmonic excitation data where the switch closes. This frequency is constrained by two points: 1) the frequency where the switch first closes and 2) the frequency where the switch opens. Using these two known points and also the known designed gap distance the MEMS switch has to travel during closure allows one to then solve the nonlinear amplification ratio Eq. 12 for the damping ratio and natural frequency.

2. Experimental Approach

The goal of the experimental approach was to empirically characterize MEMS acceleration switches on a linear impact table and an inductive shaker, and use these results to determine damping values. During an impact event, typically all modes are excited resulting in a superposition of modal displacements. During harmonic excitation, a particular mechanical mode can be excited generating a very simple motion. Damping values determined from harmonic excitation will be very specific to the mode, whereas damping values obtained from impact tests will be generalized.

There were many different parts to the experimental system setup used to test the sensors, and two MATLAB programs were written to analyze the data. A linear shock table was used to produce a high impact shock. Four channels were also used to measure each sensor one at a time. Six JFTP sensors were attached to the mounting plate and moves at high speeds into a cushion.

The harmonic excitation method used an inductive shaker with accelerometer feedback control to hold a constant acceleration value through the sine sweeps. Data acquisition records the time versus switch voltage data and correlates into frequency versus switch voltage. Switch closure is indicated by a non-zero voltage. MATLAB post-processing programs were developed to sort through each data set and obtain the relevant information needed to solve for damping and natural frequency.

2.1 Linear Shock Machine

The LSM-100 linear shock machine used pressurized air and a piston arm to pull back the plate, which compressed spring coils (Fig. 5). The piston arm would hit the trigger and release the plate, forcing the plate into a damping pad at high speeds. The trigger could be moved at different, measurable distances to vary the acceleration amplitude. Data were collected and displayed by a WinCAT Data Acquisition System (GHI Systems, Inc) when the acceleration of the plate surpassed a certain g-force threshold specified by the user.

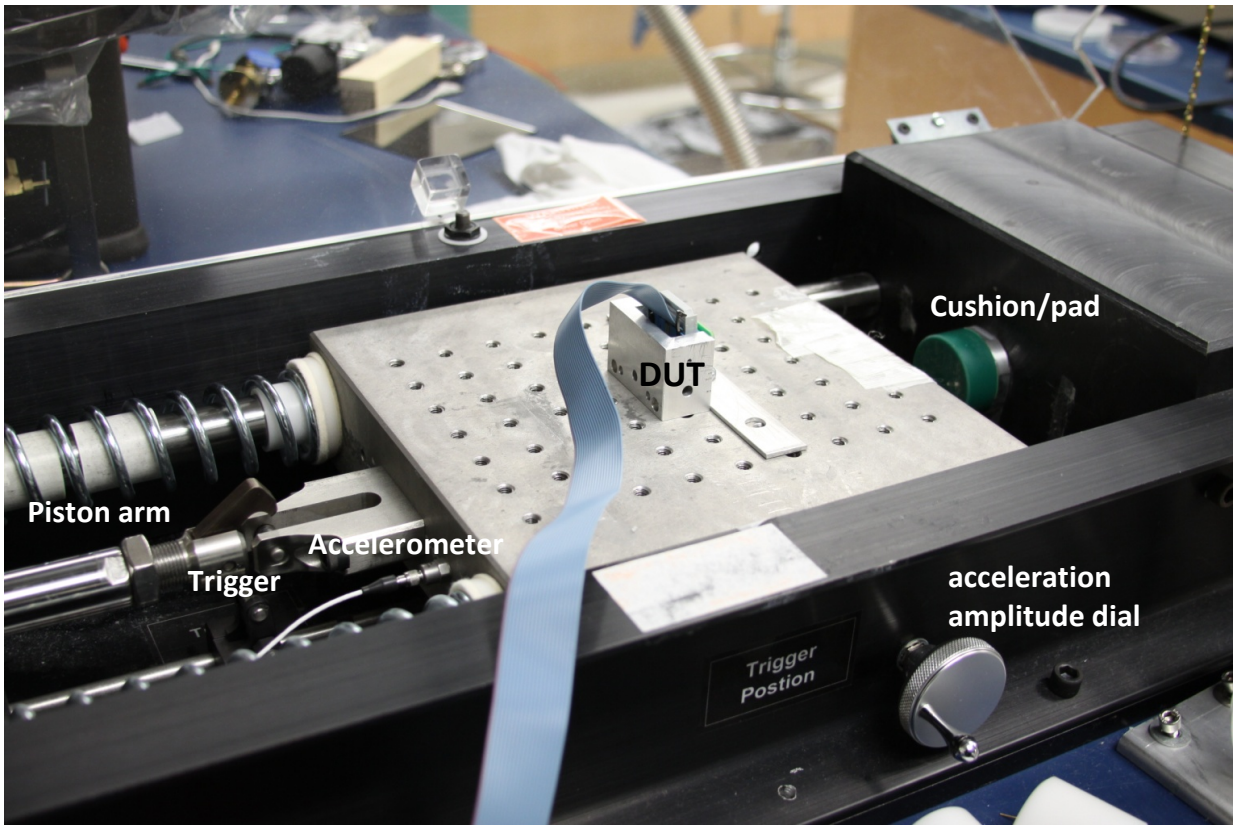

Fig. 5 Open LSM-100 linear shock machine (GHI Systems, Inc)

2.1.1 System Setup

The system setup and WinCAT software was arranged to analyze one sensor at a time. The power supply, channel input connection, and piston arm control are shown in Fig. 6. Four channels connected to the data acquisition device were used to collect data. Channel 1 was used for measuring acceleration of the table at impact and Channels 2, 3, and 4 (Fig.7) measured the voltage changes for each contact (top, in-plane, bottom). For shorter durations with the harder cushion, data were taken at a frequency of 125 kHz for a duration of 4.10 ms. For longer durations with the softer cushion, 10-bit data were taken at a frequency of 50 kHz for a time duration of 10.24 ms.

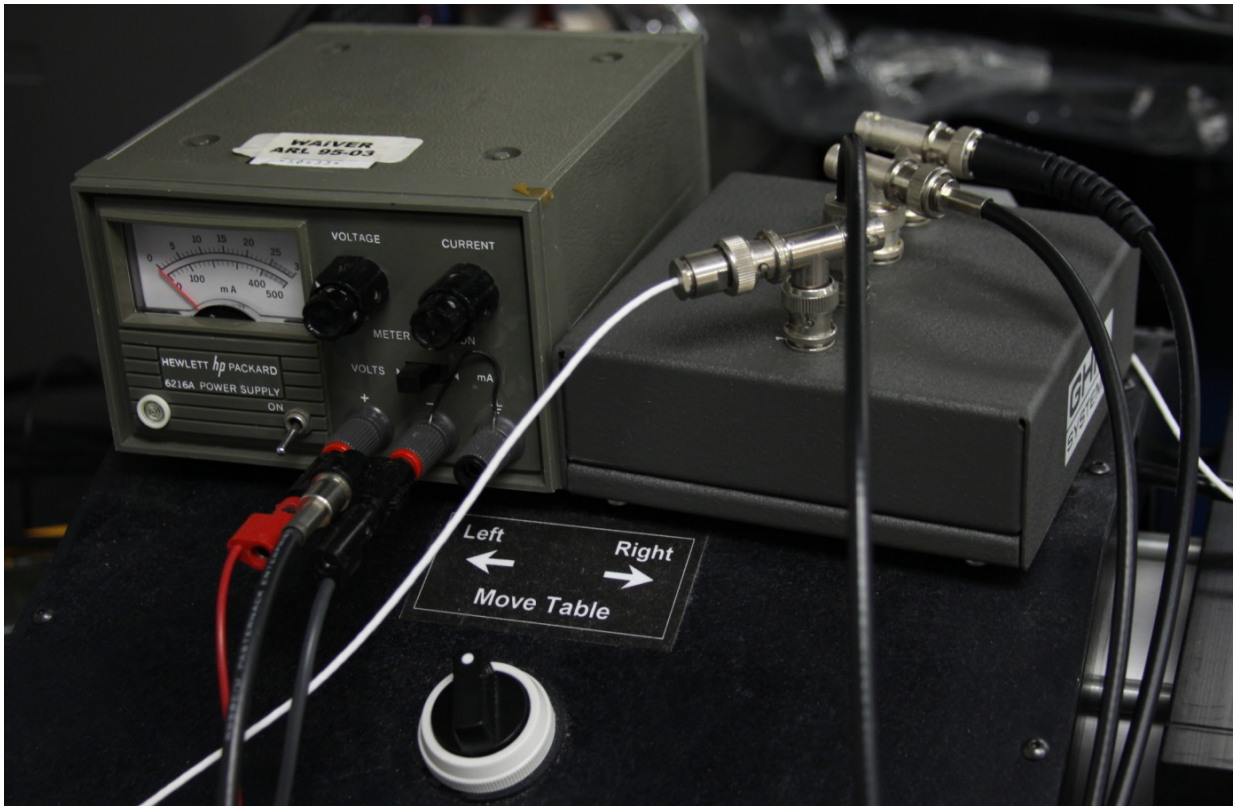

Fig. 6 Power supply (left), channel input connections (right), and piston arm control (bottom)

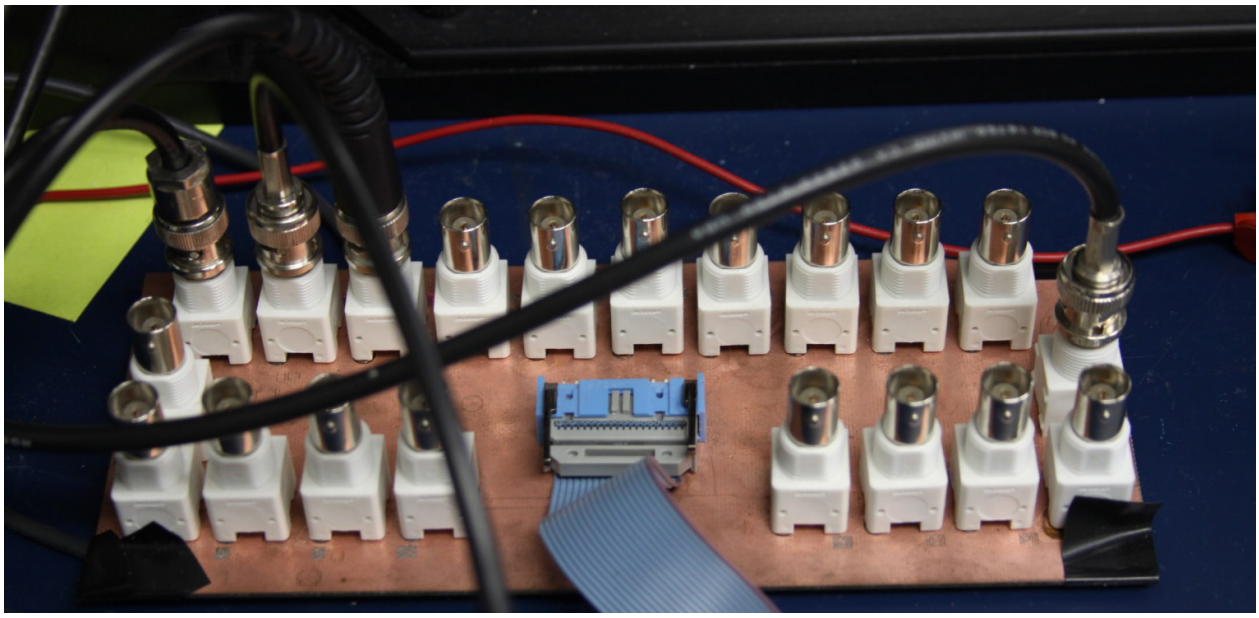

Fig. 7 Three channel (left) and power supply (right) connections

2.1.2 Sensors

Six JFTP sensors (Fig 8) were attached to a voltage divider circuit that was connected to the data acquisition device. The sensors were attached to a mounting plate in different orientations using screws and washers.

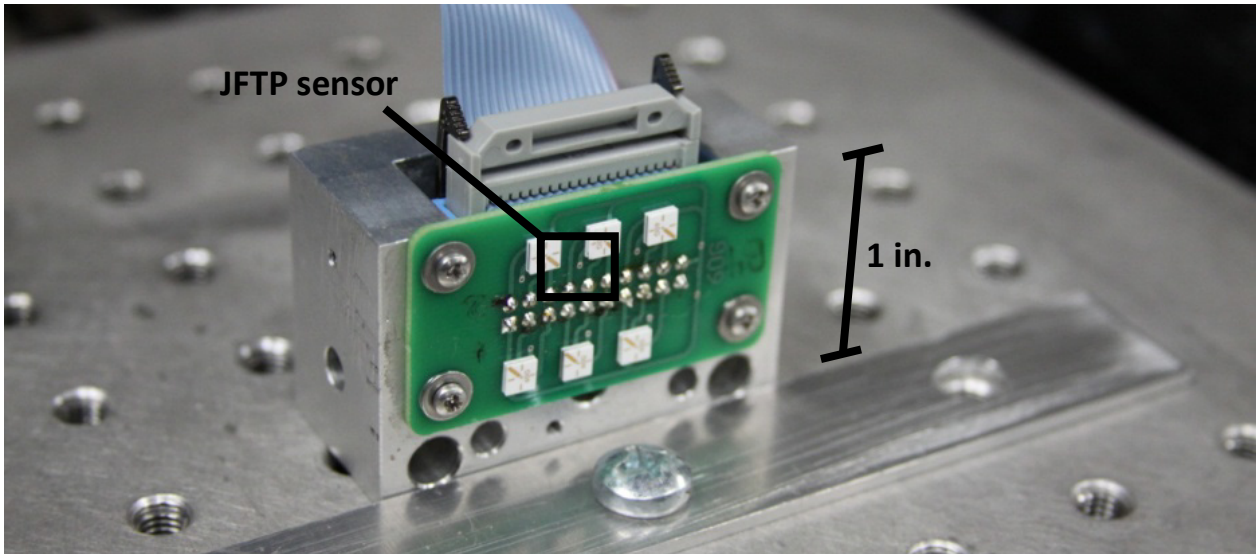

Fig. 8 Six 60G JFTP sensors attached to mounting plate

2.1.3 Impact Pads

Different pads (Fig 9) were used to absorb the shock from the impact. Softer cushions were made of rubber and the harder cushions were made of a harder plastic.

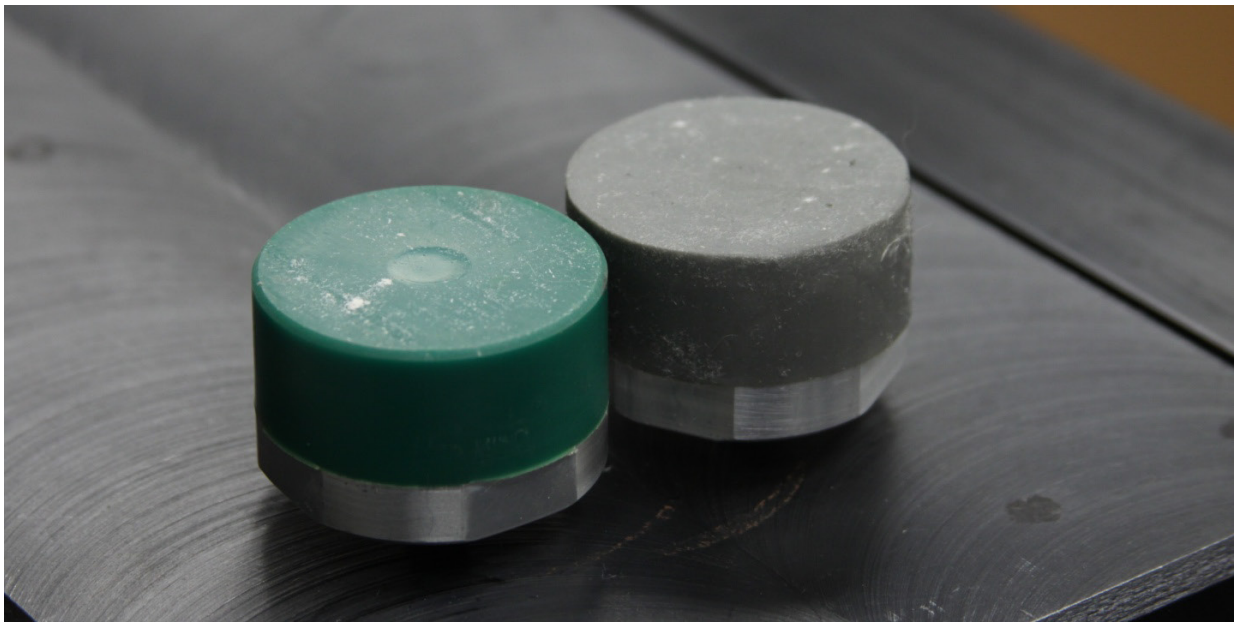

Fig. 9 Two different shock absorber pads: hard plastic (left) and soft rubber (right)

2.2 Harmonic Excitation Experimental Setup

The harmonic excitation method was conducted at the US Army Research Laboratory's (ARL) Weapons and Material Research Directorate, Ballistic Structures and Launch Dynamics Laboratory in Adelphi, Maryland. The experimental setup uses an inductive shaker controlled via a feedback accelerometer. The harmonic excitation method for modal damping characterization requires constant acceleration amplitude. The data acquisition system measures acceleration and switch voltage as a function of time and correlates these data to the driving sine sweep frequency ranging from 100 Hz–10 kHz. The data acquisition software had to be modified such that switch closure remained unfiltered during sine sweeps. Sine sweep software typically has a travelling notch filter that removes frequencies outside the sine sweep frequency.

Figure 10 illustrates the inductive shaker used (left) where the MEMS impact switch are mounted on the top of the shaker (right). The printed circuit board along with the MEMS impact switches and accelerometer (right) are mounted to the top of the shaker; power, and voltage are recorded by the data acquisition system. Figure 8 shows the circuit board developed to power the voltage dividing circuitry for each MEMS impact switch. A voltage of zero indicates an open switch, whereas a voltage of +5 V indicates a closed switch.

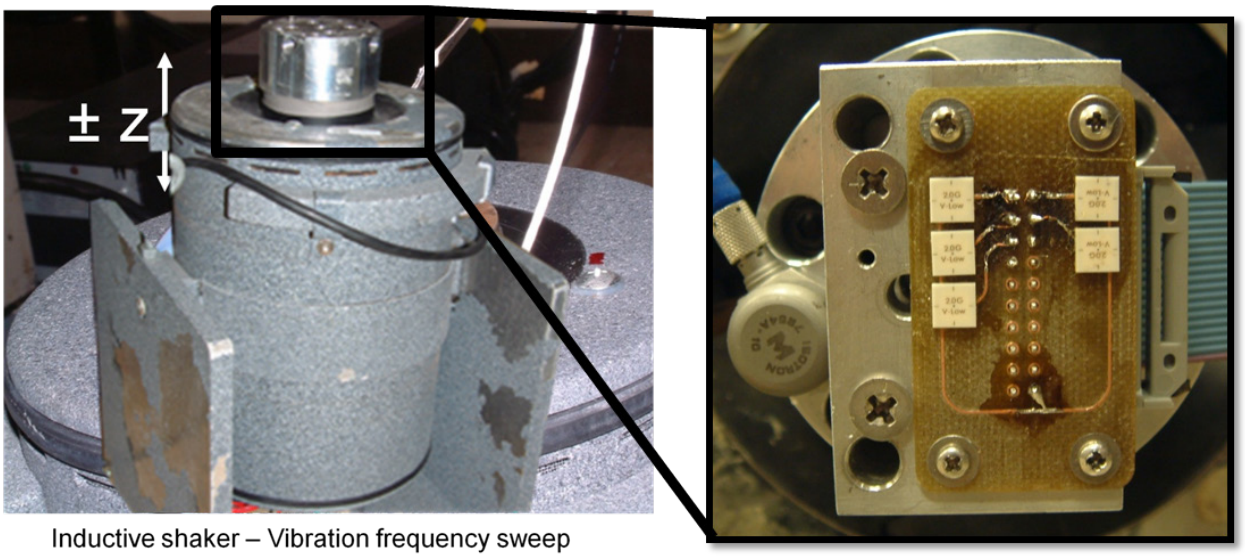

Fig. 10 Numerical method; experimental data (top) and initial calculated model (bottom)

2.3 MATLAB Programs

MATLAB programs where developed for each testing method describe in Section 2. The first described MATLAB program uses empirical acceleration table results and modeling a second-order-differential-equation fit to mimic the MEMS acceleration switch response. This method iteratively adjusts the damping ratio until the solution converges.

The second method uses harmonic vibration empirical data to solve the amplification ratio equation for both natural frequency and damping. The MEMS acceleration switch is vibrated at an amplitude where the switch begins to make closure at its natural frequency. The frequency span where switch closure first occurs and finally opens are the ends points for solving a nonlinear amplification ratio equation. This method is constrained to solve only underdamped systems; however, it is more advantageous when quantifying single modal damping values rather than impact excitation where many modes are excited.

2.3.1 MATLAB Programs – Impact Table Damping Model

MATLAB programs were written for both a numerical and an analytical method. The numerical method guessed some damping value and used an ordered differential equation solver (`ode45`) to determine a time of closure at the gap distance between the proof mass and the contact. If the calculated closure time did not match the closure time in the data, the program would estimate a closer value of damping using the relationship

$$\zeta_n = \zeta_{n-1}(1 - Kt_{n-1}) \tag{16}$$

where k is a refinement factor. The analytical method used the `fzero` function and applied it to the real part of the solution of the equation of motion by setting the whole function to zero. The

program calculated the damping using the gap distance between the proof mass and the contact and the experimental closure time.

An example of the convergence method is portrayed in Figs. 11 and 12. In Fig. 11, a graph of actual experimental data for a single test is shown as well as the model for the calculated acceleration input. The switch closes the gap when the displacement is 30 µm. The incorrect damping value in the switch empirical data shows that switch closure happens at a later time, so damping is continually increased until the time closure value matches that of the original. In Fig. 12, the code converged to a final damping value at 2.041 after 42 iterations, changing the damping by a factor of 5.

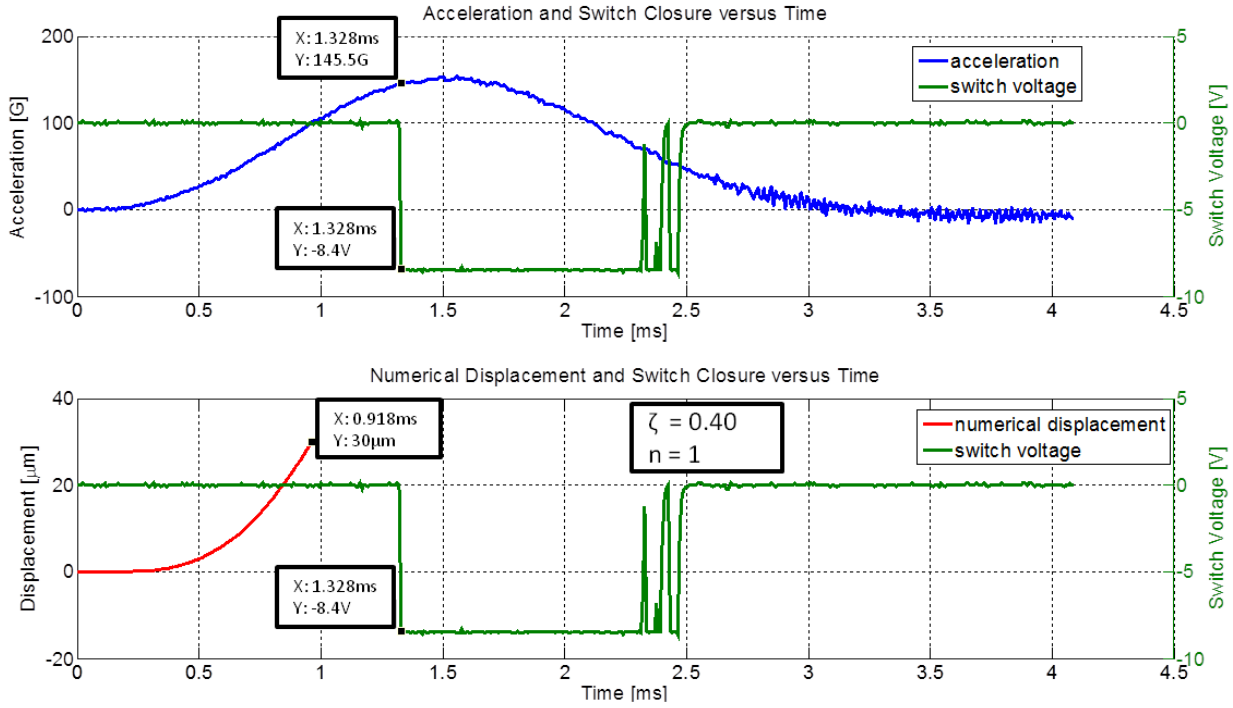

Fig. 11 Numerical method; experimental data (top) and initial calculated model (bottom)

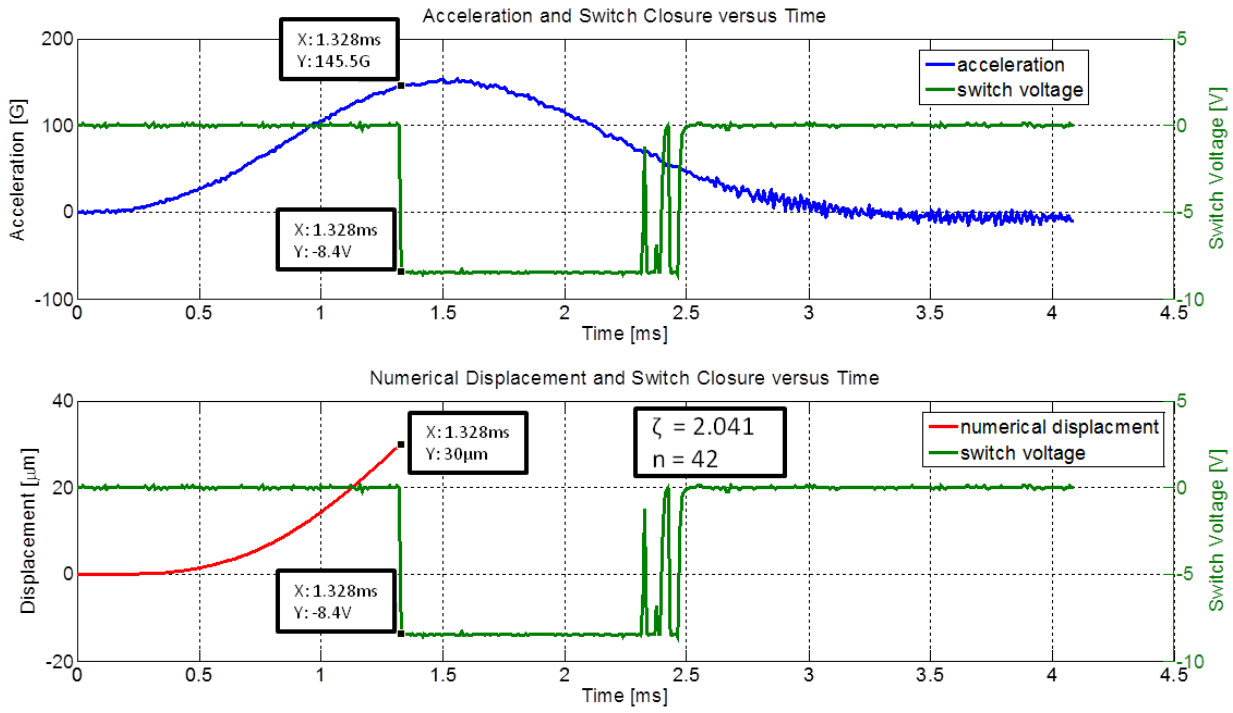

Fig. 12 Numerical method; experimental data (top) and final calculated model (bottom)

2.3.2 MATLAB Programs – Harmonic Excitation Modal Damping Predictor

A well-known method to measure damping for harmonic excitation is by directly measuring displacement and correlating that to the input displacement to produce an amplification ratio as a function of frequency. If input acceleration is held constant, then the input displacement amplitude is proportion to inverse of frequency squared. Therefore at higher frequencies, less input displacement is needed to produce a constant acceleration. Figure 13 illustrates that if output displacement is known for various excitation frequencies then the quality factor and damping of the system can be directly determined. However, in the case of MEMS acceleration switches, the peak value of the amplification ratio is unknown because of switch closure.

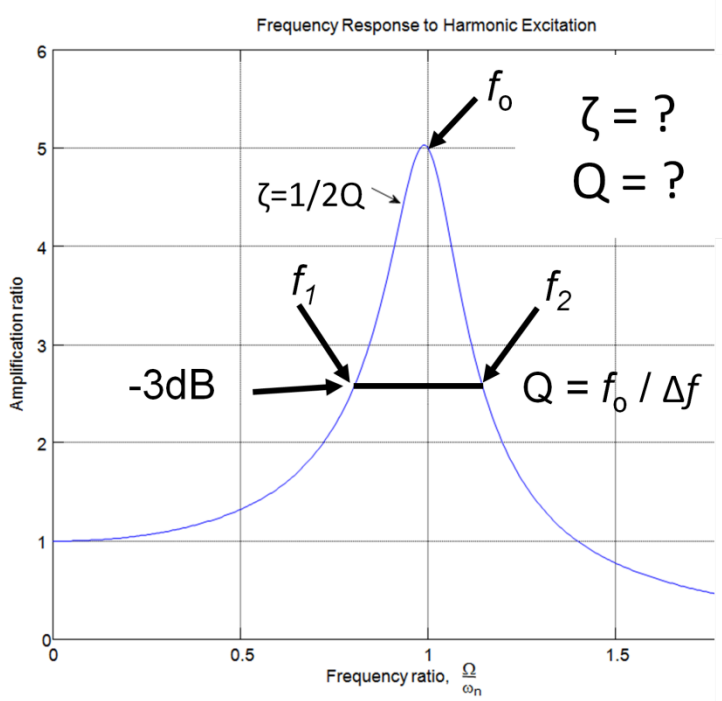

Fig. 13 The –3 dB method to quantify the quality factor and damping of a mechanical system.

Figure 14 illustrates that switch closure only indicates the frequency at which the switch closes and then subsequently opens (left). Thus, the only information attained is the two frequency values where the switch first closes and then opens and the input displacement, which is input acceleration amplitude divided by the frequency squared. In the case of Fig. 14 (right), these values are 0.7395 and 1.094 (non-dimensional frequency).

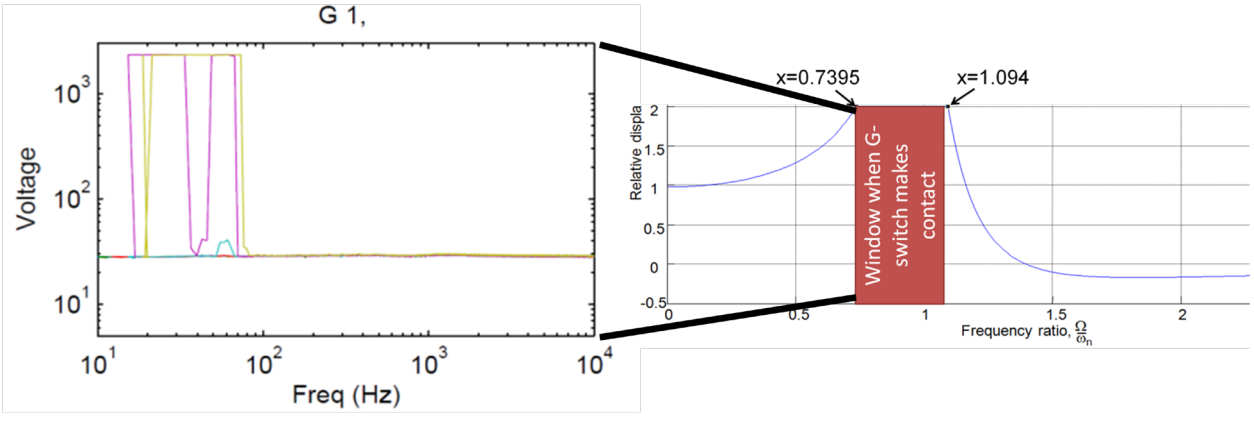

Fig. 14 Switch voltage as a function of frequency (left) and the information retain from an amplification ratio standpoint (right)

The values shown in Figs. 14–15 are used below as an example to calculate the damping ratio and natural frequency of MEMS acceleration switches when all that is known is switch closure and open frequencies and input acceleration. Input displacement is determined by dividing the constant input acceleration value by the closure and opening frequencies which gives two values that Eq. 12 can be solved. MATLAB's built-in function `fsolve` can be used to solve a system of nonlinear equations (e.g., 17 and 18).

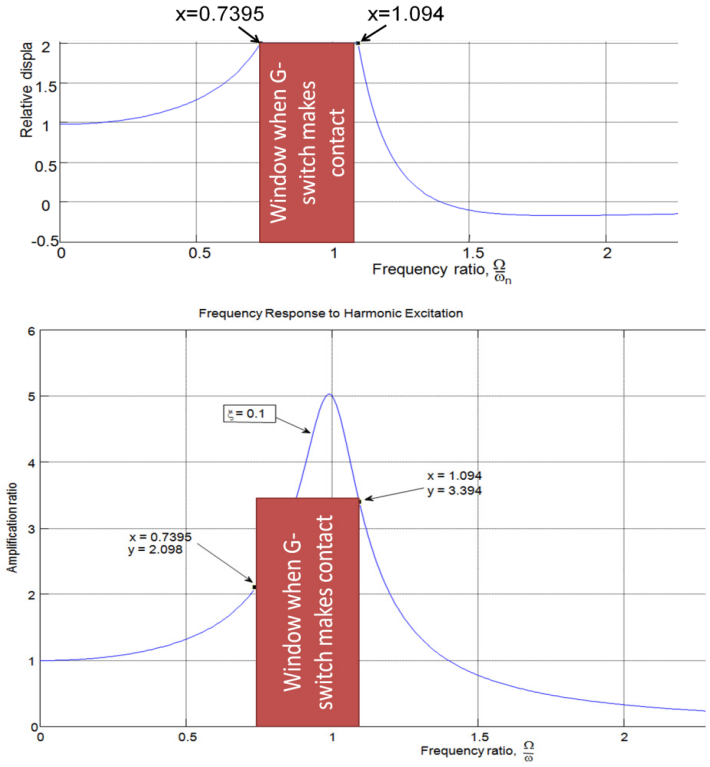

Fig. 15 Switch voltage as a function of frequency (top) and the closure frequency window plotted on top of a frequency response graph that assume a 0.1 damping ratio (bottom)

$$\ddot{x}(t) = A_o \sin(\Omega t)$$

$$x(t) = \frac{-A_o}{\Omega_{1,2}^{\,2}} \sin(\Omega_{1,2} t)$$

A_o = acceleration amplitude (constant)

$\Omega_{1,2}$ = shaker frequency at switch closure

Gap distance = displacement at closure

$$x(t) = \frac{-A_o}{\Omega^2} \sin(\Omega t)$$

Gap distance = x_o

$$Amp = \frac{x_o}{x\left(t_{\Omega_{1,2}}\right)}$$

$$\frac{x_o}{x\left(t_{\Omega_{1,2}}\right)} = 2.098 = \frac{1}{\sqrt{\left[1-\left(\frac{\Omega_1}{\omega_n}\right)^2\right]^2 + \left(\frac{2\varsigma\Omega_1}{\omega_n}\right)^2}} \quad (17)$$

$$\frac{x_o}{x\left(t_{\Omega_{1,2}}\right)} = 3.394 = \frac{1}{\sqrt{\left[1-\left(\frac{\Omega_2}{\omega_n}\right)^2\right]^2 + \left(\frac{2\varsigma\Omega_2}{\omega_n}\right)^2}} \quad (18)$$

)

3. Results and Discussion

Data were obtained for MEMS acceleration switches using the two methods defined in the Section 2. Results from the linear impact table and harmonic excitations method are organized and discussed. The linear impact table method uses acceleration shock profile to induce MEMS acceleration switch closure. This method differs from the harmonic excitation method because when the MEMS switch is put into a transient shock environment multiple modes are excited. The harmonic excitation method uses an inductive shaker to excite single modes of interest. The harmonic excitation method only works for an underdamped system, which is a limiting factor for this developed testing method. Both testing methods revealed nonlinearity to damping as a function of input amplitude. This is due to squeeze-film effects amplifying as a function of response velocity and gap closure.

3.1 Impact Table Damping Results

Damping is expected to change in a manner related to the change in velocity of the impact test. This is expected due to gap closure of the MEMS acceleration switch. The value of the squeeze-film constant, Eq. 14, increases as gap distance decreases and input frequency increases. Both the analytical method and the numerical analysis method were expected to result in similarly consistent values for the in-plane contacts. Using both methods, the damping coefficient for top contact movement was expected to be consistently higher than in-plane damping.

The analytical method for calculating damping was too sensitive to input variations; the acceleration, closure time, and frequency produced impractical damping values when applied to the equation. Additionally, manufacturers closure gap tolerances are thought to be inconsistent and have a fairly large standard deviation. Static centrifuge testing needs to be conducted to determine what the acceleration closure value is for each orientation—determining this will give better insight on how the gap distances vary.

The numerical method proved to be a better way of determining damping because the analytical method used many assumptions when solving the characteristic equation. One assumption was that the system was an underdamped system, so any cases of overdamped or critically damped systems would be inaccurately modeled using the equations of motion.

In Figs. 16 and 17, there is a general decreasing acceleration pattern over increasing closure time for both contacts. There are data points that show constant peak acceleration over different closure times.

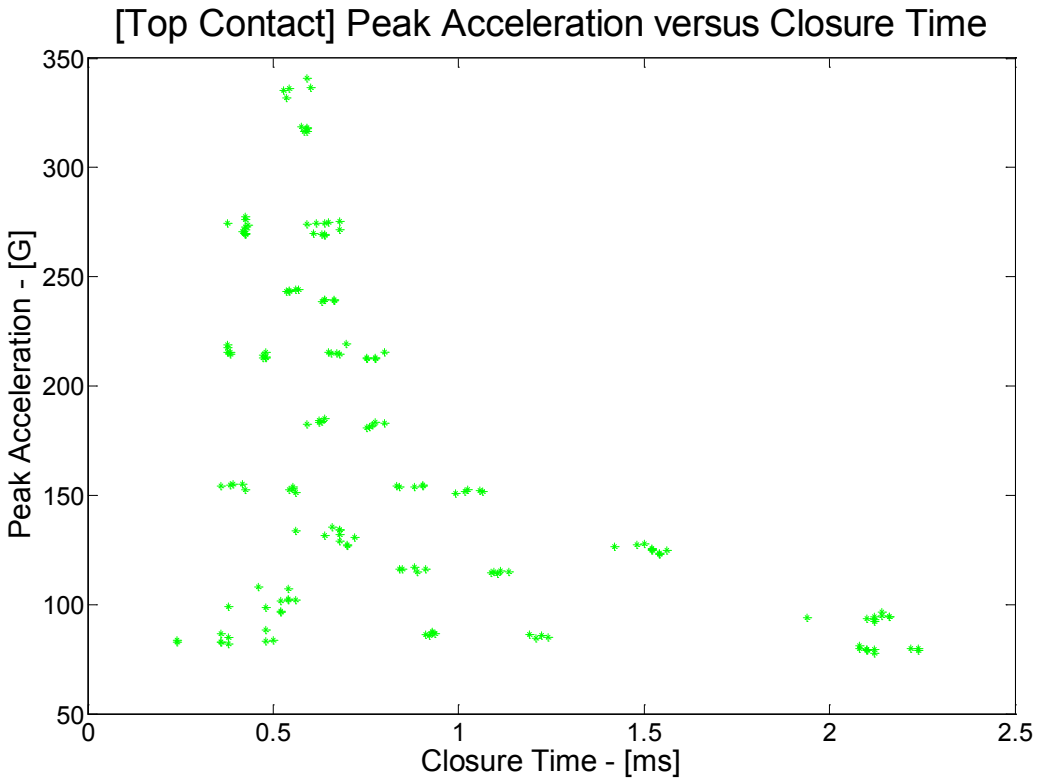

Fig. 16 (Top contact) peak acceleration vs. closure time

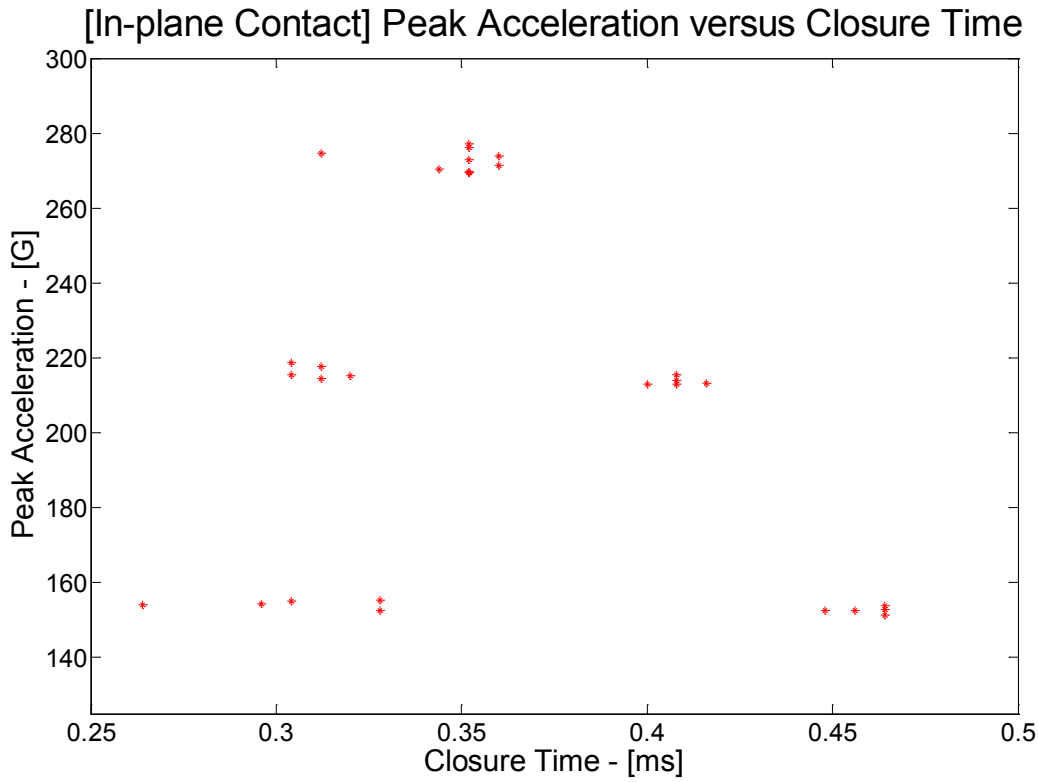

Fig. 17 (In-plane contact) peak acceleration vs. closure time

Two or three outliers above a damping value of three were considered anomalies and were most likely due to the proof mass bouncing around or chattering inside the sensor and aliasing due to the 125-kHz sampling frequency for data acquisition, seemingly increasing closure time.

Similar patterns occur with damping as with acceleration. In Figs. 18 and 19, there is a general decreasing damping pattern over increasing closure time for both contacts, but there are patterns of constant peak acceleration over different closure times. The top contact damping was always extremely high and had inflated damping values. There seemed to be cases of overdamping because the calculated squeeze-film factor was extremely large.

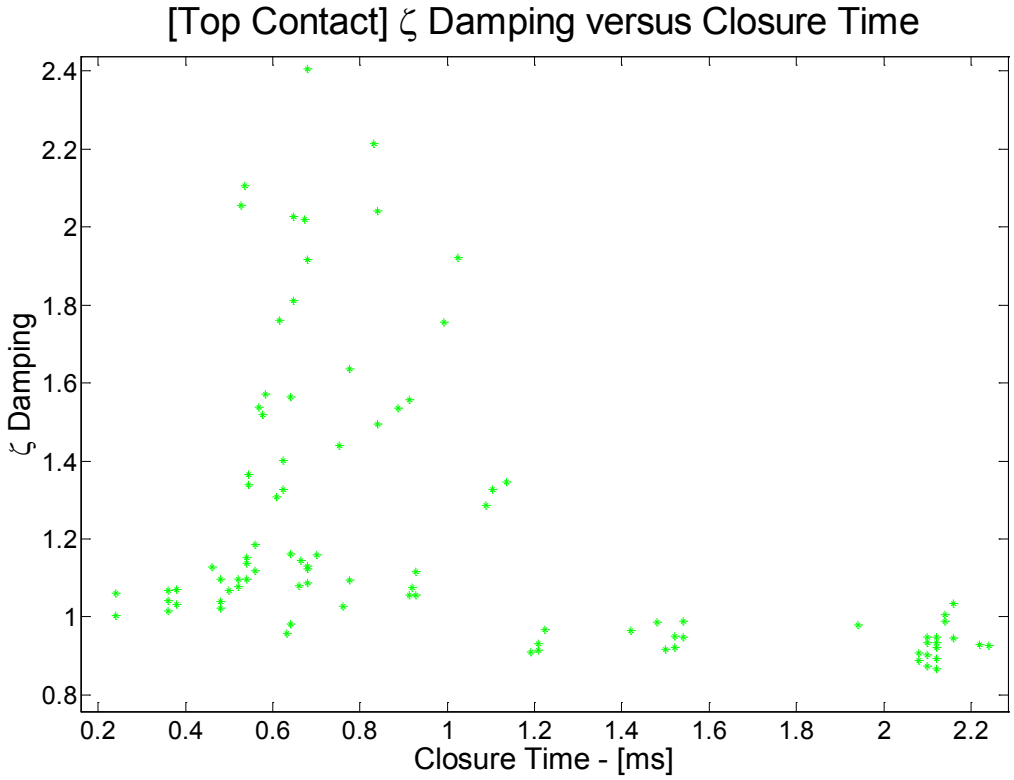

Fig. 18 (Top contact) damping vs. closure time

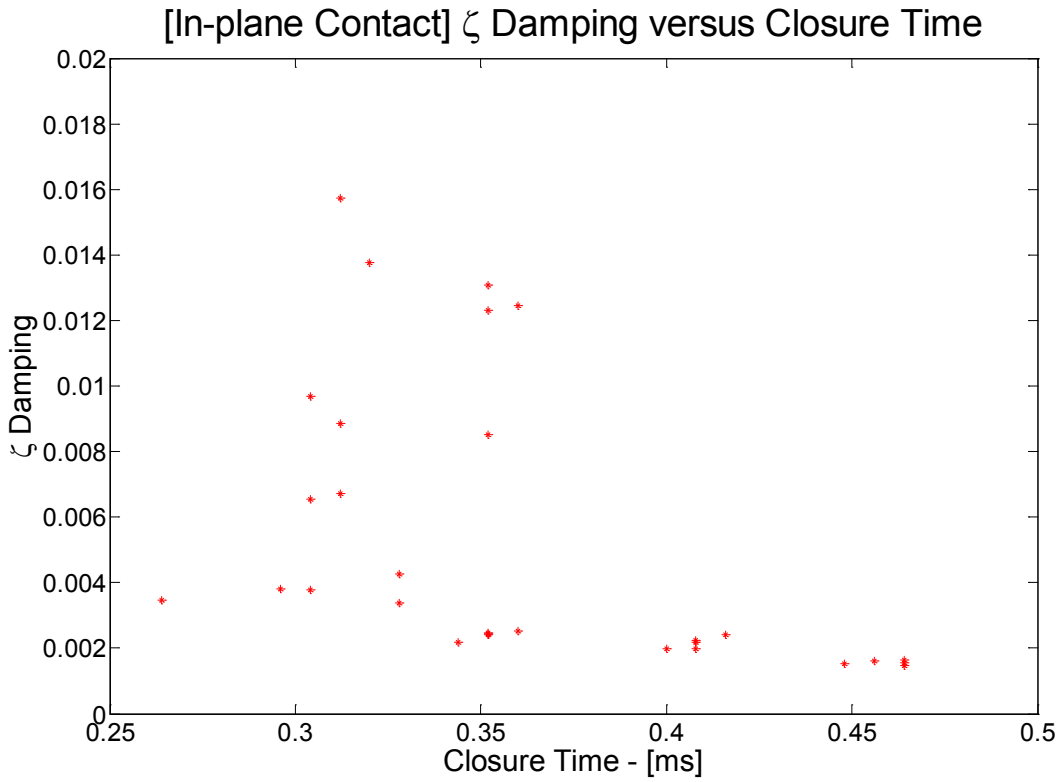

Fig. 19 (In-plane contact) damping vs. closure time

In Fig. 20, the top contact damping values are inflated due to high squeeze-film damping. For both contacts (Figs. 20 and 21), there are clear patterns of increasing damping with increasing peak acceleration.

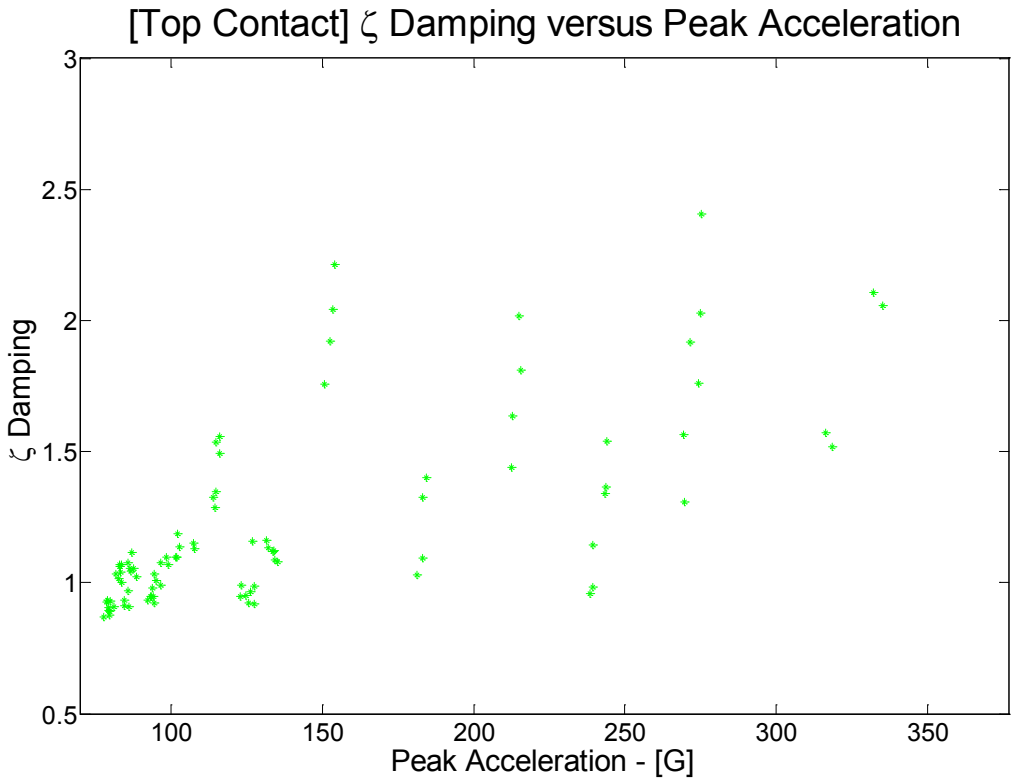

Fig. 20 (Top contact) damping vs. peak acceleration

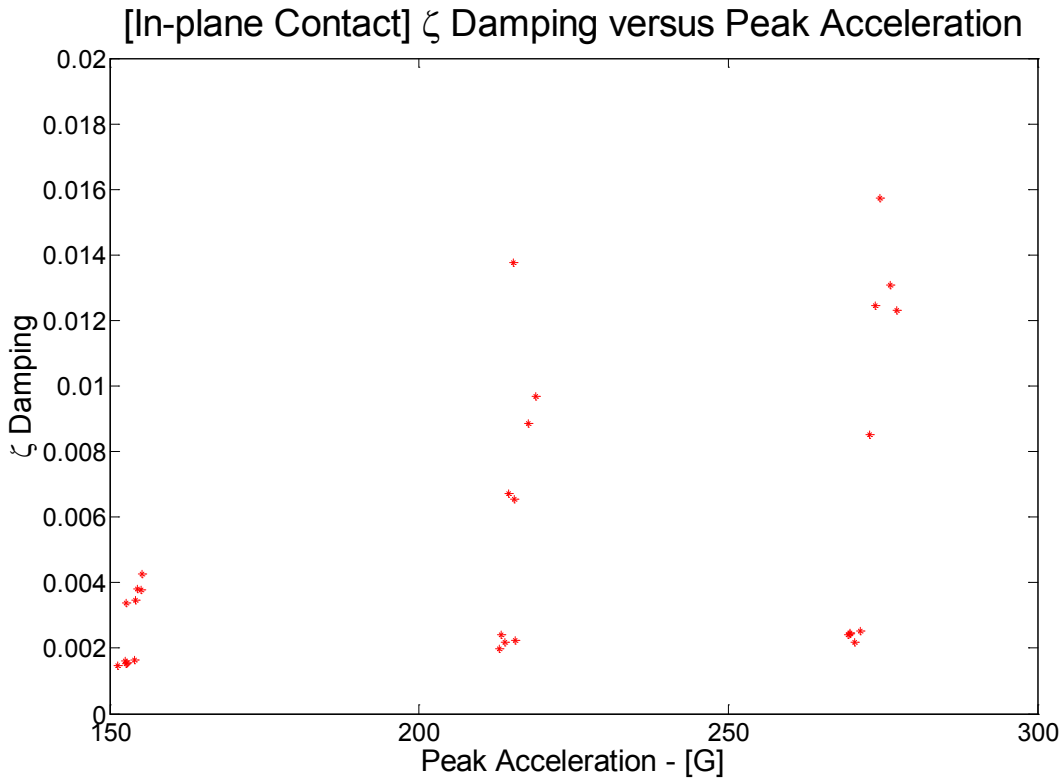

Fig. 21 (In-plane contact) damping vs. peak acceleration

A relationship of increasing damping with increasing velocity is portrayed in Figs. 22 and 23. The relationship between damping and velocity were due to the drag force in the system. This pattern also accounts for the relationship between damping and acceleration for the same time value. The values for damping were inflated or inaccurate due to the sampling frequency and large squeeze-film values. These factors severely impacted the calculated damping coefficients, but there were clear relationships shown in the results.

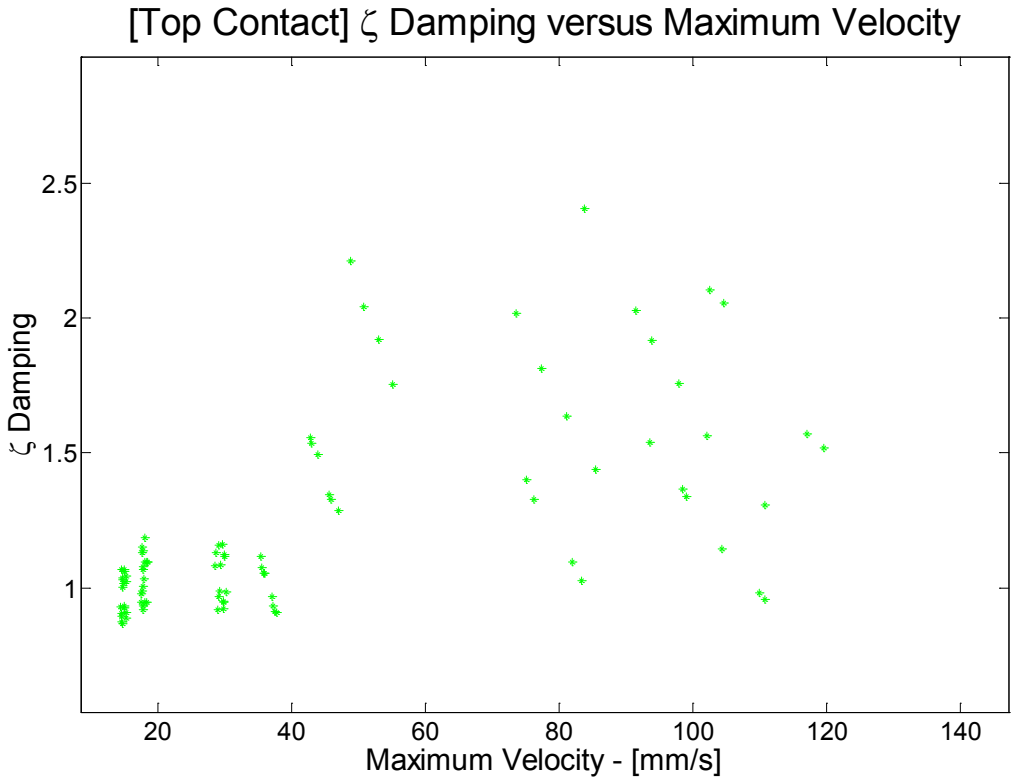

Fig. 22 (Top contact) damping vs. maximum velocity

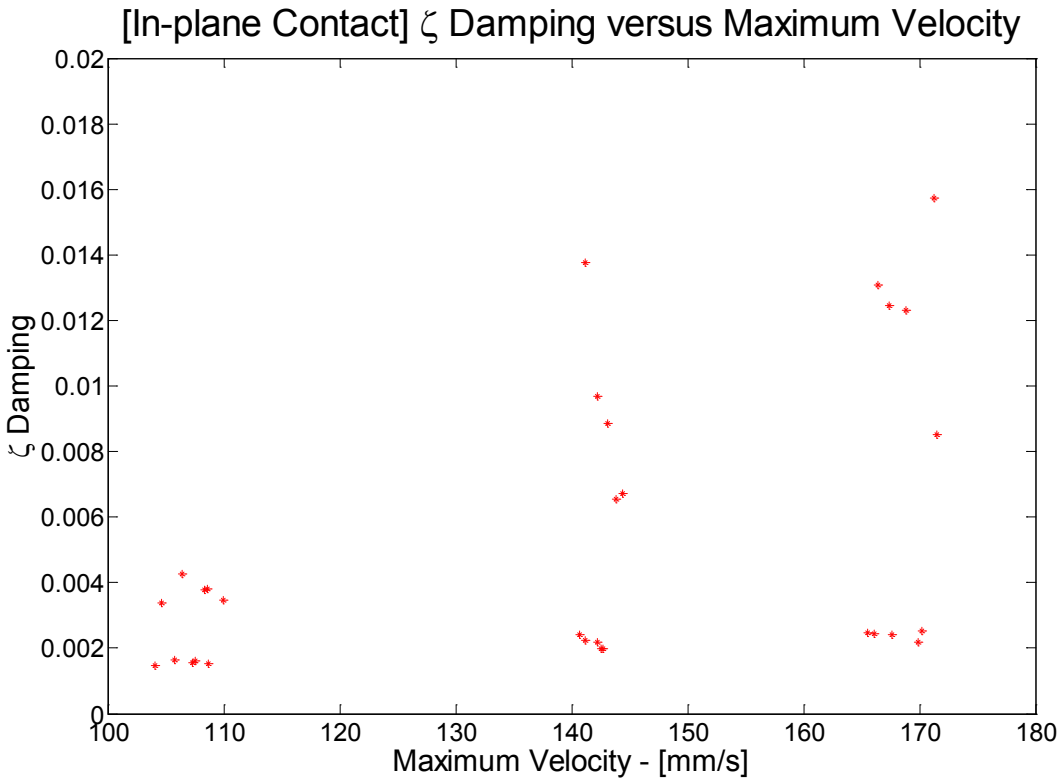

Fig. 23 (In-plane contact) damping vs. maximum velocity

3.2 Harmonic Excitation Modal Damping Results

The damping results from the harmonic excitation method are shown in Tables 1 and 2 for 50G and 500G MEMS acceleration switches. When first comparing the side (in-plane) and out-of-plane (top and bottom) damping values, the results were unexpected. However, upon further review of the contact surface area, the side contact had roughly two times surface area as the out-of-plane (top and bottom) contacts. Squeeze-film damping would be more pronounced in the side contact rather than the top or bottom since it has double the contact surface area.

Since the top and bottom contacts are inherently identical, the difference in damping values are attributed to the manufacturing gap tolerance for the top and bottom contact distances. The static acceleration switching threshold may deviate as much as 10% for the top and bottom contacts, indicating variation in the gap distances as a result of different acceleration threshold values.

The data in Tables 1and 2 are for fairly low input acceleration amplitude ranging from 5–10G's. Switch ringing was seen at input acceleration amplitudes greater than 20G's, where lateral switch contact was sensed. This is believed to be from contact happening at such a great velocity the switch rings, exciting other modes lateral to the input acceleration direction. Larger input acceleration amplitudes often resulted in higher damping values, which are not shown in Tables 1 and 2. This is believed to be attributed to velocity dependent damping effects that were also seen during the impact table damping characterization tests.

Table 1 The 50G MEMS acceleration switch – results, 5–10G amplitude excitation

Mode #/Shape	FEA modal (Hz)	Contact	Freq	Damping
Mode 2 / Out-plane	680	Top	653.9312	0.004161
Mode 2 / Out-plane	680	Bottom	735.2356	0.005367
Mode 3-4 / In-plane	798	Side	802.6671	0.044097

Table 2 The 500G MEMS acceleration switch - results, 5–10G amplitude excitation

Mode #/Shape	FEA modal (Hz)	Contact	Freq	Damping
Mode 2 / Out-plane	2156	Top	2719.009	0.004860
Mode 2 / Out-plane	2156	Bottom	2703.846	0.001689
Mode 3-4 / In-plane	2482	Side	2817.224	0.009231
Mode 3-4 / In-plane	2482	Spin	3216.026	0.000007

4. Conclusions

For MEMS systems and systems characterized by low Reynolds numbers, the damping force of bodies moving in a fluid has been found to be linearly proportional to the speed of the mass.[11] This relationship is determined through analyzing the drag force, which is proportional to the velocity and damping of the system. In plotting the maximum velocity against the calculated damping coefficients, the results support the correlation and show a steady increase in damping with increasing velocity. This shows that damping may be quantified as a function of velocity $\zeta_n(\dot{x})$. The pattern of decreasing damping with increasing closure time can therefore be explained with an increasing drag force for larger velocity and damping values. This pattern similarly accounts for increasing damping with increasing acceleration; higher peak acceleration within the same time duration causes a greater maximum velocity.

Time-closure values may also have been aliased due to the frequency at which data were taken. The proof mass bouncing around in the sensor was an unmeasurable and uncontrollable factor in the data, so time-closure values may have been incorrectly obtained from the data. The bouncing also may have closed the switch with other contacts, causing the MATLAB code to incorrectly read the proper closure time for the correct contact.

The switching threshold was set to 0.79 V, which may have affected the time-closure data. In the event of bouncing or almost incomplete closure, the switching threshold may not have been exceeded and the data for time of closure may have been missed and resulted in subsequent closure being detected thus greatly increasing measured closure time.

In the future, a more accurate convergence algorithm may be required to more efficiently converge on the correct damping value. In addition, an increase in sampling frequency would

more accurately detect closure, which would provide more accurate data to be analyzed. The inflated values for the top contact could be lessened if gap-dependent squeeze-film value model was used. The squeeze-film constant in Bao[3] was derived using a small amplitude of vibration assumption at a set gap distance and doesn't take into account a reducing gap that goes to zero.

Determining the damping values of an impact acceleration switch helps categorize how the switch functions. Factors such as mass and spring constants are tailorable and measurable, but the majority of the damping is caused by the mechanical switch's interaction with the N_2 packaged gas environment. The novel method developed to measure damping by measuring closure time helps model designs to further improve design to more accurately close at the expected acceleration.

5. References

1. Muldavin JB, Rebeiz GM. Nonlinear electro-mechanical modeling of MEMS switches. Microwave Symposium Digest, 2001 IEEE MTT-S International. May 2001;3:2119–2122.
2. Li G, Hughes H. Review of viscous damping in micromachined structures. Proc. SPIE 4176, Micromachined Devices and Components VI, August 2000.
3. Bao M, Yang H. Squeeze film air damping in MEMS. Sensors and Actuators A. 2007;136:3–27.
4. Glynne-Jones PM, Tudor J, Beeby SP, White NM. An electromagnetic, vibration-powered generator for intelligent sensor systems. Sensors and Actuators A: Physical. February 2004;110(1–3):344–349.
5. Williams CB, Yates RB. Analysis of a micro-electric generator for Microsystems. Sensors and Actuators A: Physical. April 1996;52(1–3):8–11.
6. Brotz J. Damping in CMOS-MEMS resonators. MS Thesis, ECE, Carnegie Mellon University, June 2004.
7. Gorelick S, Dekker JR, Leivo M, Kantojärvi U. Air damping of oscillating MEMS structures: modeling and comparison with experiment. COMSOL Conference 2013, VTT Technical Research Centre of Finland, 2013.
8. Zhang W. Energy dissipations in MEMS resonators: fluid damping of flexural resonators and thermoelastic damping. Doctoral dissertation, University of California, Santa Barbara, UMI 3245943, December 2006.
9. Steeneken PG, Rijks Th.GSM, van Beek JTM, Ulenaers MJE, De Coster JR. Puers R. Dynamics and squeeze film gas damping of a capacitive RF MEMS switch. Journal of Micromechanics and Microengineering. 2005;15:176–184.
10. Mohite SS, Kesari H, Sonti VR, Pratap R. Analytical solutions for the stiffness and damping coefficients of squeeze films in MEMS devices with perforated back plates. Journal of Micromechanics and Microengineering. 2005;15:2083–2092.
11. Younis MI. MEMS Linear and Nonlinear Statics and Dynamics. Springer, New York, NY, 2011.

List of Symbols, Abbreviations, and Acronyms

ARL	US Army Research Laboratory
CAD	computer-aided design
DUT	device under test
HEMDP	harmonic excitation modal damping predictor
JFTP	Joint Fuze Technology Program
MEMS	microelectromechanical system
A	area of the plate (m^2)
F	driving force (N)
K	refinement factor
R	coefficient of the steady state solution (m)
c	damping
c_1 , c_2	coefficients of the terms of the transient solution
k	spring constant (N/m)
$k_e(\sigma)$	coefficient of the elastic damping force
l	characteristic length of the plate (m)
m	mass (kg)
P_a	ambient pressure (Pa)
t	time (s)
ζ	damping coefficient
η	is the aspect ratio of the plate (for a square plate, $\eta = 1$)
μ	coefficient of viscosity of the fluid (Pa-s)
σ	squeeze number

ω	harmonic frequency ($\mathrm{rad/s}$)
ω_d	damping frequency ($\mathrm{rad/s}$)
ω_n	natural frequency ($\mathrm{rad/s}$)

1 DEFENSE TECHNICAL
(PDF) INFORMATION CTR
DTIC OCA

2 DIRECTOR
(PDFS) US ARMY RESEARCH LAB
RDRL CIO LL
IMAL HRA MAIL & RECORDS MGMT

1 GOVT PRINTG OFC
(PDF) A MALHOTRA

2 DIRECTOR
(PDFS) US ARMY RESEARCH LAB
RDRL SER L
RYAN KNIGHT
EVAN CHENG

INTENTIONALLY LEFT BLANK.